MSc in Photonics

PHOTONICS**BCN**

Universitat Politècnica de Catalunya (UPC)
Universitat Autònoma de Barcelona (UAB)
Universitat de Barcelona (UB)
Institut de Ciències Fotòniques (ICFO)

http://www.photonicsbcn.eu

Master in Photonics

MASTER THESIS WORK

EXPLORING NbTiN SUPERCONDUCTING SINGLE PHOTON DETECTORS WITH QUANTUM DETECTOR TOMOGRAPHY

Juan Carlos Rivera Hernández

Supervised by Dr. Michiel J. A. de Dood, Leiden Institute of Physics, Leiden University, The Netherlands
Co-supervised by Dr. Crina Cojocaru, UPC

Presented on date 9th September 2019

Registered at

Escola Tècnica Superior d'Enginyeria de Telecomunicació de Barcelona

Exploring NbTiN superconducting single photon detectors with quantum detector tomography

Juan Carlos Rivera Hernández

Escola Tècnica Superior Superior d'Enginyeria de Telecomunicació de Barcelona, Universitat Politècnica de Catalunya, Campus Nord, Carrer de Jordi Girona, Barcelona, 08034, Spain with Erasmus mobility at Leiden Institute of Physics, Leiden University, Niels Bohrweg 2, 2333 CA Leiden, The Netherlands

E-mail: 4jcrivera3@gmail.com

Abstract. The optical response of NbTiN superconducting single photon detectors is studied using quantum detector tomography which separates the detector response in single and multiple photon contributions. Three different NbTiN nanodetectors of 70, 100 and 150 nm width are compared based on their detector tomography curves. The energy dependent photon response for the 100 nm nanodetector at two different wavelengths is explored. The detectors present a non-linear behaviour, which complicates the comparison. For the first time, we find that tomography curves saturate above a certain bias current and we compare the current density required to achieve the single photon regime.

Keywords: superconducting single photon detectors, nanowire, quantum detector tomography, superconductivity.

1. Introduction

Superconductive single photon detectors (SSPDs) consist of a few nanometer thin and ∼100 nm wide superconducting nanowire made of strongly disordered superconducting material with a low electron density [1]. Commercial devices feature a long meandering wire ∼500 μm to create an active area comparable to a diffraction limited spot size of the incident light, e.g. the mode size of a single-mode fiber at 1550 nm wavelength. When these wires are current biased close to the device critical current, the energy of a single photon is enough to break superconductivity and creates a voltage pulse that can be amplified and detected. Superconductive detectors have several practical advantages [2] when compared to other single photon detectors. Contrary to semiconductor based detectors, SSPDs are not limited by the band gap of the material allowing to detect single photons infrared wavelengths [3]. Compared to other technologies SSPDs present lower dark counts rate, nanosecond reset time and picosecond timing jitter. It should be noted, however, that not all these properties can be optimized simultaneously.

These characteristics establish SSPDs as a key technology for several future quantum applications. However, there is still a long way to go, since the detection mechanism is not fully understood. In particular the step after the absorption of a photon, leading to a macroscopic resistance that creates a perceptible voltage pulse, is still debated and is believed to depend on the material and dimensions of the nanowire. There are several models available in literature that try to explain the detection mechanism [4]. The underlying explanation of all the models is the following: Absorption of a single photon destroys Cooper pairs in the superconductor

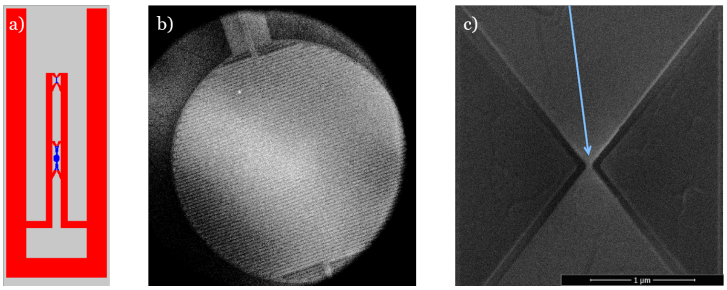

Figure 1. NbTiN nanodetector structure. (a) Design of the whole nanodetector. The red areas in the mask are removed during the fabrication process. The upper and lower blue areas correspond to the constriction and to the inductor, respectively. (b) Scanning electronic microscope (SEM) image of the inductor, illustrating its meander structure. (c) SEM image showing the 100 nm wide constriction.

creating a localized zone, i.e. a hotbelt or hotspot [5], where the wire is either in the normal state or in a state of weakened superconductivity. Depending on the bias current a normal region is formed with a macroscopic resistance. This normal region is not self-sustaining under voltage bias conditions [6, 7] and the wire eventually self resets and returns to its original state generating a voltage pulse during the process.

In this work, three NbTiN SSPDs of 70, 100 and 150 nm width are considered. The nanodetectors are fabricated on a single substrate with a 13 nm thick NbTiN film to facilitate a direct comparison. The film is deposited on a silicon substrate with a ∼270 nm thick thermal oxide layer. The oxide layer electrically isolates the detector from the substrates and serves to optimize photon absorption for a wavelength of 1550 nm. The geometry of the nanodetector was first suggested and developed by Bitauld et al. [8]. An SEM image of one of the NbTiN nanodetectors used in this work is presented in figure 1. Each device consists of long 500 nm wide, meandering wire that serves as a large inductor, typically of 500 nH, and the nanofabricated constriction itself, where the photon detection takes place.

Because the mechanism of detection is not fully understood characterizing the optical response of these nanodetectors is not straightforward and cannot be expressed in terms of a single efficiency. Instead the characterization involves quantifying the multi-photon contributions. Quantum detector tomography (QDT) [9, 10, 11] allows measurement of the detection probabilities in the photon number basis of a detector whose optical response is unknown. Analyzing the QDT performance gives additional insight by separating the physical process of photon absorption from the probabilities p_i to create a click when i photons are absorbed.

Before characterizing the detectors, we first explain the basics of the QDT process in more detail. The goal of QDT is to find the probability of a particular detection outcome given that n photons are incident on the detector. In the case of SSPDs we assume that there are only two possible events after the absorption of a photon, click or no-click, i.e. the voltage pulse does not contain information about the number of absorbed photons. Furthermore, to probe these photon counting statistics, a collection of known quantum states of light is used. The detector is probed sufficiently many times with each state to accurately determine the probability of each possible experimental outcome. Preferably QDT uses coherent states of lights since the probability distribution of photons in the coherent states is well-known and characterized only by the mean number of photons per laser pulse. Once the probability of each outcome is measured, it is possible to determine the probability of each outcome given a certain number of incoming photons. We use the fact that the distribution of the absorbed photons is also a coherent state

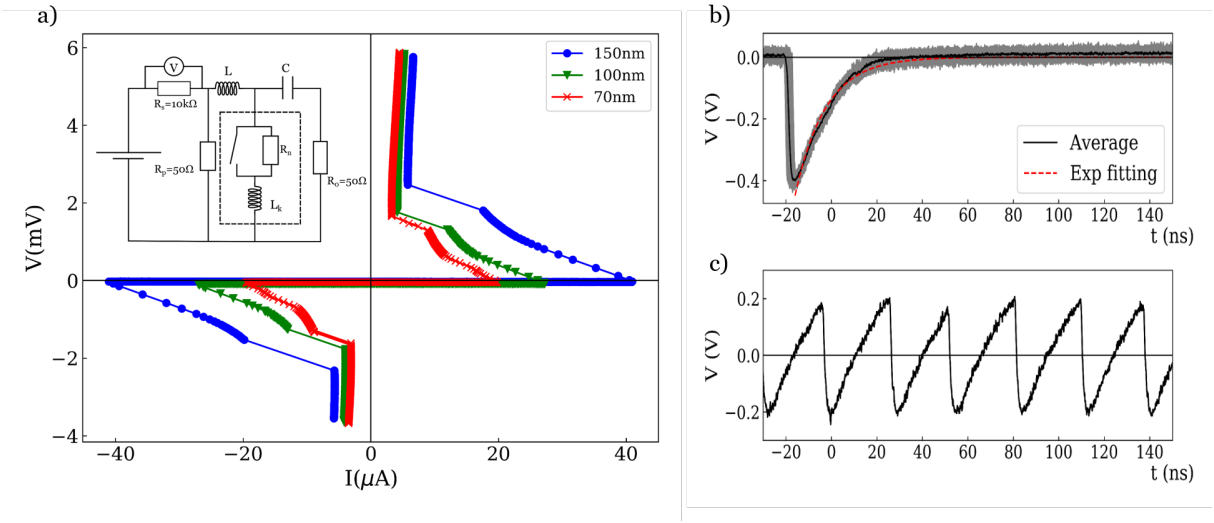

Figure 2. (a) I-V characteristics of the three NbTiN detectors at T=4.0K. Inset: Schematic of the electronic circuit used to bias the SSPDs. (b) Voltage pulse of a detection event, averaged over 100 pulses (black line). The grey lines represents all the individual events. The red dashed line is an exponential fit giving $L_k = 672$ nH. (c) Relaxation oscillations observed in the regime where the detector is biased beyond the critical current.

with the average number of absorbed photons being a factor η smaller than the incident photons. Taking these factors into account, the probability that the detector clicks is given by:

$$R_{click} = 1 - e^{-\eta N} \sum_{i=0}^{M} (1 - p_i) \frac{(\eta N)^i}{i!}, \tag{1}$$

where N is the mean photon number per laser pulse in the input beam, η represents the overall efficiency of the detection process, the p_i represent the probability of a detector click when exactly i photons are absorbed and M reflects the fact that at high powers the detector saturates ($p_i = 1$ for $i \geq M$) [12]. Consequently, η and the set of p_i are the parameters that completely define the response of a photo-detector.

The aim of this work is to characterize and compare NbTiN nanodetectors of different width. This is carried out through QDT, which allows to separate the probability that a photon is absorbed, given by η, from the one photon detection probability p_1. We anticipate that a direct comparison between the nanodetectors is best done by comparing the probabilities p_i.

2. Experimental

The NbTiN SSPDs are placed inside a closed-cycle cryostat with free-space optical access with the samples kept at a constant temperature of 4 K. The samples are voltage biased following the circuit represented in figure 2(a). The bias current is applied via computer controlled and low-noise voltage source (Yokogawa GS2000) and via a bias-T (Mini-circuits ZNBT-60-1W) schematically represented by the L and C in the circuit. The electronics inside the dashed box represent an equivalent circuit of the SSPD. As mentioned before, the absorption of a photon breaks the superconductivity, which correspond to the switch opening, at which time the detector acquires a resistance R_n. With the given bias circuit the wire is now voltage biased and the current decays until the self-heating of the wire is sufficiently reduced so that the wire becomes superconductive again. As a result the switch closes and the current reaches its original

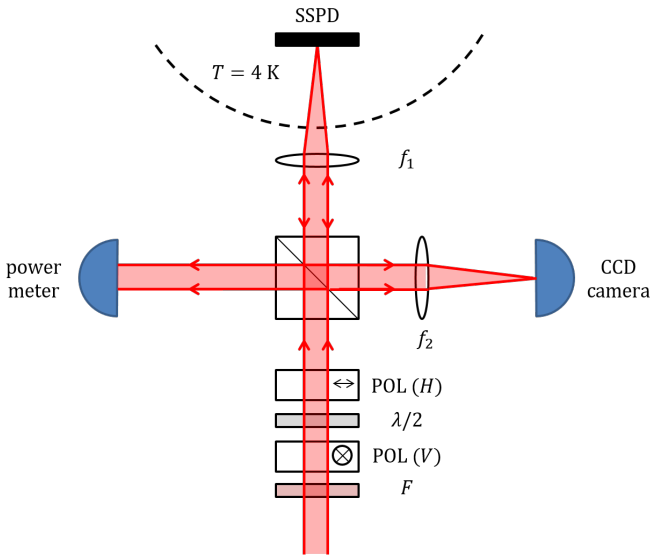

Figure 3. Schematic drawing of the optical setup used for detector tomography. The incident light is passed through a bandpass filter (F) and the power is tuned using a combination of two crossed polarizers and a motorized $\lambda/2$ plate. The detector is placed inside the cryostat at $T = 4$ K. A non-polarizing beam splitter is used to monitor the power and to be able to create an image of the laser spot and the sample using lenses with focal length $f_1 = 125$ mm and $f_2 = 250$ mm.

value with a time constant which depends on the kinetic inductance (L_k) of the device [7, 13]. The shape of a voltage pulse after amplification using a combination of two identical amplifiers (Mini-Circuits ZFL-1000LN) is presented in figure 2(b).

Three different regimes can be observed in the I-V characteristics of the NbTiN nanodetectors given in figure 2. The horizontal part of the curves in figure 2(a) corresponds to the superconductive regime where no measurable voltage difference over the nanowire as a function of bias current is observed. The steep region for voltages above +2 mV and below -2 mV corresponds to permanent resistive state of the device characterized by a self-heating hotspot [6, 14]. In between there is a transition regime where the detector presents a switching behaviour between the superconductive and normal states. In this region the so called relaxation oscillations [15] take place, giving periodic pulse trains (figure 2(c)). For larger values of R_p the devices irreversibly jump directly from the superconductive to the resistive state. This effect is called latching [14, 15] and prohibits the self-reset mechanism that is essential for a properly working SSPD. In order to avoid latching R_p should be sufficiently low. We experimentally determined that a value fixed to 50 Ω suffices.

Detector tomography experiments were performed using a pulsed white-light continuum source (Fianium). This source has a repetition rate of 20 MHz and creates pulses of the order of 20 ps. Laser light at a center wavelength of 780 nm and a full-width-at-half-maximum of 10 nm is selected using a bandpass filter. Undesired wavelengths are filtered out before this bandpass filter using a combination of dichroic mirrors, shortpass and longpass filters. In order to be able to properly perform QDT a wide dynamic range of powers is needed. To achieve this the input power on the SSPD is tuned using a half wave plate between two perfectly crossed high quality Glan-Thompson linear polarizers (B. Halle) as shown in figure 3. This optical setup allows to reach up to 5 orders of magnitude tunability in power. A 50/50 non-polarizing beam splitter is placed before the sample to reflect part of the light towards a power meter that monitors

the incident power on the detector. The backwards reflected light from the sample is directed towards a CCD camera to create an image of the detector and the laser spot. This image is used for coarse alignment of the setup.

3. Results and discussion

The first step in the detector tomography procedure is to explore the optical response of the detector as a function of the bias current. The measured count rate as a function of bias current is shown in figure 4 for four different incident powers. The results show that for low bias current almost no photons are detected since their energy is not enough to trigger the detection mechanism. As can be seen in the figure, when the bias current increases towards the critical current, the number of detected photons increases and rapidly reaches a saturation, for high powers, where almost every sent pulse is detected. These measurements show that the number of detected photons does not grow proportional to the incident power. Instead, the detector shows a non-linear behaviour of the count rate of the NbTiN nanodetectors as a function of both incident power and bias current.

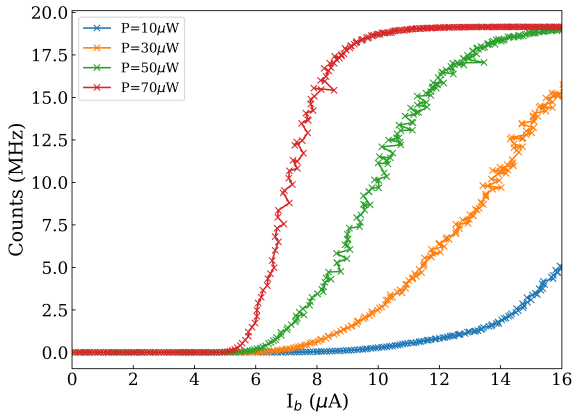

Figure 4. Measured count rate R_{click} as a function of bias current (I_b) for several input powers on the 100 nm wide NbTiN detector.

Tomography curves represented as measured count rate as a function of incident power for the three detectors are presented in figure 5. A variety of curves is presented for different bias currents. The slope of these tomography curves on a log-log scale is intimately related to the number of photons involved in the detection process [1]. For a detector that is sensitive to n photons the count rate as a function of power is proportional to P^n. As expected, for low bias currents the slope of the curves is steeper indicating that multiple photon contributions are predominant. As the bias current increases towards the critical current of the device the one photon contribution becomes more and more relevant and the slope of the tomography curve tends to 1. It should be noted that the tomography procedure allows to analyze curves that have a non-integer value of the slope by quantifying the contributions from different photon numbers.

The data for these new NbTiN nanodetectors show that for high bias currents, the tomography curves have the same shape but they are shifted horizontally. For the highest currents the tomography curves show near perfect overlap. This strongly suggests that the one photon detection probability p_1 is saturating to one. This is an important observation because these measurements comprise the first data set where saturation is observed in the tomography of a nanodetector.

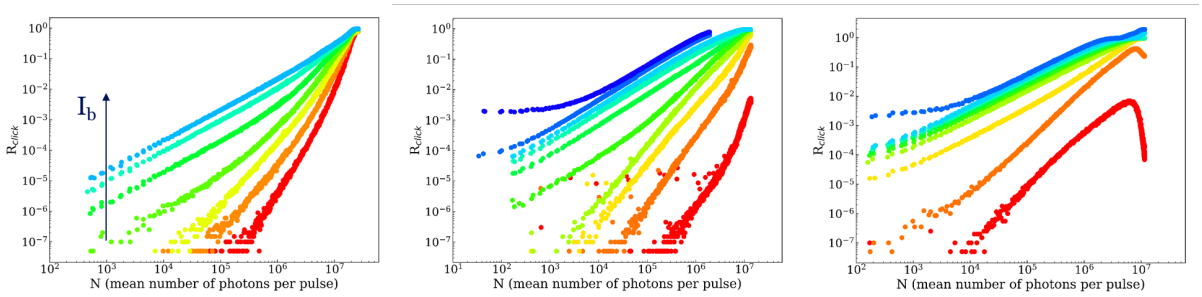

Figure 5. Detection probability per pulse R_{click} as a function of the mean number of photons per pulse normalized to the laser repetition rate of 20 MHz for the three NbTiN detectors. For each detector a variety of curves for different bias current is shown. (a) 150 nm. (b) 100 nm. (c) 70 nm.

This saturation is most clearly observed for the 100 nm and 70 nm wide constriction (Figures 5(b) and 5(c)). Surprisingly, for the 150 nm detector neither the one photon regime nor the tomography saturation are clearly observed. In addition the tomography curves for the 70 nm detector present strange behaviour at higher powers and lower bias currents. Under these conditions the count rates decrease with increasing power. We hypothesize that this drop in count rate is either due to heating of the detector by the optical power or due to driving the detector in a new regime of relaxation oscillations induced by the incident power. This hypothesis could be further explored by varying the repetition rate of the laser. Unfortunately, this is not possible with the current super-continuum source.

To illustrate the tomography process figure 6 shows two measured tomography curves (symbols), at different bias currents of 11.7 μA and 14.3 μA together with the tomography fit (solid line through the symbols). Although, the two curves present a rather different shape, both curves show a saturation of the detection rate at high powers. Tomography at the lower bias current (figure 6(a)) contains contributions from different photon numbers. The contributions from the different photon numbers are indicated by the different curves under the tomography data. Curves are included for the one photon (green), two photon (red) and higher number of photons processes (purple). As can be seen in the figure the data for $I_b = 11.7\mu$A shows a distinct kink that indicates the transition between the one and two-photon regimes. In contrast, the data for the higher bias current (figure 6(b)) does not show a distinct kink in the curve. Since the energy of a single photon is enough to trigger the detection mechanism, the one photon detection process is the most dominant contribution until saturation of the count rate sets in at click probabilities above 0.1 ($> 10^6$ photons per pulse).

Although detector tomography can be successfully performed on each of the nanodetectors a direct comparison remains difficult. The most obvious way to compare detectors of different width is to compare measurements done at the same current density. However, large quantitative differences are found between the detectors making a comparison between three different detectors not feasible.

Instead to perform the comparison between the different NbTiN detectors, two curves with similar tomography fit parameters are selected. The current density for the detectors can then be calculated leading to a pairwise comparison. The values are presented in table 1. The efficiency η is excluded from the analysis. Typical values of η are 1-4$\cdot 10^{-7}$ and are consistent with the area of the nanodetector compared to the laser spot size. In our experiments, we find that the exact value depends strongly on the optical alignment making a direct comparison of η not relevant.

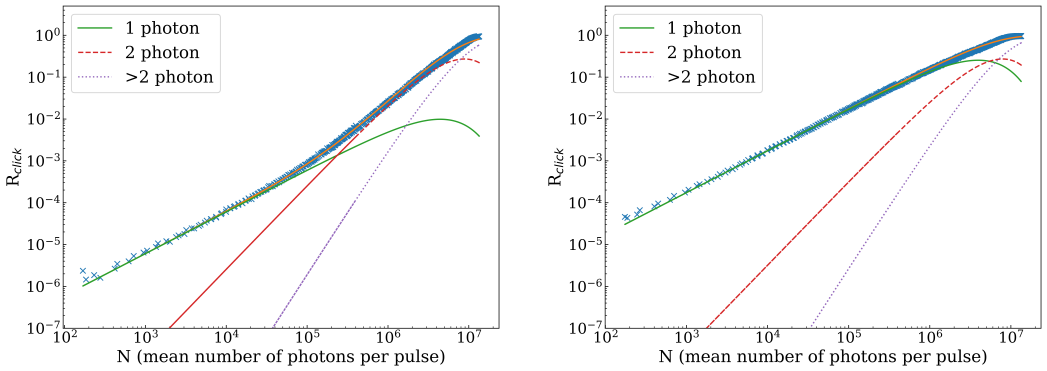

(a) (b)

Figure 6. Detector click probability R_{click} as a function of the mean number of photons per pulse for the 100 nm wide NbTiN nanodetector. The solid yellow line through the data points is the fit of the full tomography equation, showing a successful tomographic reconstruction of the observed count rates. The green (solid) and red (dashed) lines show the one and two photon contribution to the count rate, respectively. The dotted violet line shows the contribution of higher number of photons. The curves were measured for two different bias current. (a) I_b = 11.7 μA. (b) I_b = 14.3 μA.

Table 1. Current density and tomography parameters values for the 70, 100 and 150 nm wide NbTiN nanodetectors.

	70 nm	100 nm	150 nm			
j_c (mA/μm^2)	10.1	14.0	21.0			
j_b (mA/μm^2)	–	6.7	12.9	$p_1 = 0.15$	p_2 =0.26	$p_3 = 1$
j_b/j_c	–	0.48	0.61			
j_b (mA/μm^2)	5.7	7.3	–	$p_1 = 0.67$	$p_2 = 1$	$p_3 = 1$
j_b/j_c	0.56	0.52	–			

The results of table 1 show that the current density to achieve an equivalent detector performance is closer to the critical current density as the width of the nanodetectors increases, i.e. wider detectors are less efficient at a similar current density. In addition we observe that narrow nanodetectors behave better as a true single photon detector with only η and p_1 to be determined. These observations are consistent with the detection model of photon assisted vortex entry [4, 10, 12]. The photon assisted vortex entry model would lead to a similar performance of narrow wires once the wire becomes more narrow than a specific width. For NbN this width is given by the diffusion length of quasi-particles [10, 12] and predicts similar performance for wires below 100 nm width that only depends on the current density. A closer look at the current density values reported in table 1 reveals unexpected large differences in current density for similar performance.

A more thorough analysis is performed on the 100 nm NbTiN nanodetector because the tomography curves themselves show interesting saturation behaviour at high enough bias currents. Figure 7 shows two tomography curves with a typical horizontal shift as the bias current increases. The linear dependence on a log-log scale and the fact that the shape of the curves is very similar indicates that both detectors operate in the single photon regime. The horizontal shift is then a signature of a change in the probability p_1. Performing QDT and

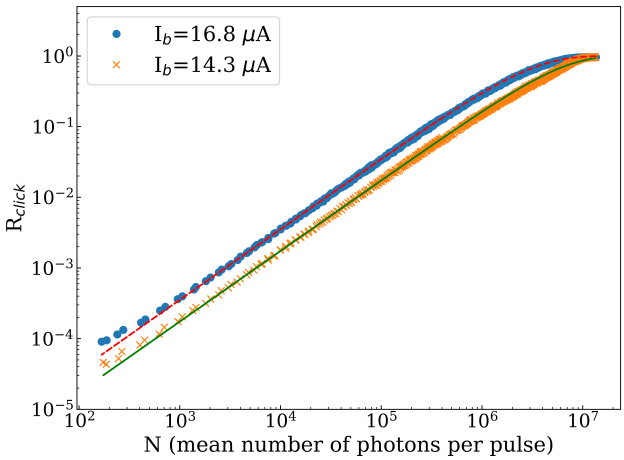

Figure 7. Saturation of the detector tomography curves for the probability rate as a function of the mean number of photons per pulse on the 100 nm wide NbTiN nanodetector. Curves are shown for two bias currents corresponding to $p_1 = 0.69$ and $p_1 = 0.99$.

analyzing the parameters of the fit, it is indeed observed that, for the yellow curve, p_1 is equal to 0.69, while for the blue curve p_1 increases to 0.99. At a wavelength of 780 nm the saturation of the tomography ($p_1 \approx 1.0$) occurs for a bias current of 16.8 μA. A further increase in bias current does not alter the tomography curves as the probability saturates at $p_1 = 1.0$. This is an interesting result as it comprises a first experimental demonstration of saturation of the internal efficiency of a nanodetector. Using the saturated curve, the absorption efficiency η is the only fit parameter because all p_i equal 1 and the efficiency η related to photon absorption does not depend on bias current.

Further insight in the operation of an SSPD and the underlying photon detection model can be obtained by studying the response for different photon energies. To this end, we explore the energy dependent photon response for the 100 nm nanodetector by comparing the response at two different wavelengths. By changing the bandpass filter, the center wavelength of the laser light is changed from 780 nm to 880 nm. Contrary to the results reported in literature for MoSi SSPDs consisting of meander structures [16], there is no simple horizontal shift in the observed count rate as a function of bias current. This is due to the fact that our NbTiN nanodetectors show a non-linear behavior that depends on both bias current and laser power. Contrary to the results of Caloz et al. [16] it is not possible in our case to identify a linear regime of photon detection and a simple comparison on raw experimental data is not possible. Instead, a full tomography study is needed in order to compare the optical response of the 100 nm detector for different wavelengths.

Selected tomography curves for the two different wavelengths are show in figure 8 for high bias current (17.1 μA, figure (a)) and lower bias current (11.1 μA, figure (b)). At high bias current the shape of the curves is nearly identical and only differ by a horizontal shift. Surprisingly, it appears as if the detector is more efficient at 880 nm wavelength as the click rate at similar powers is higher for 880 nm when compared to 780 nm. However, it should be kept in mind that the shape of the curve is determined by the values of p_i, while a horizontal shift of the curve is due to a change in the absorption efficiency. The thickness of the substrate of the device is designed to optimize the photon absorption for a wavelength of 1550 nm. Then, a change in the wavelength is intimately related with the absorption efficiency producing this horizontal shift in the tomography curve.

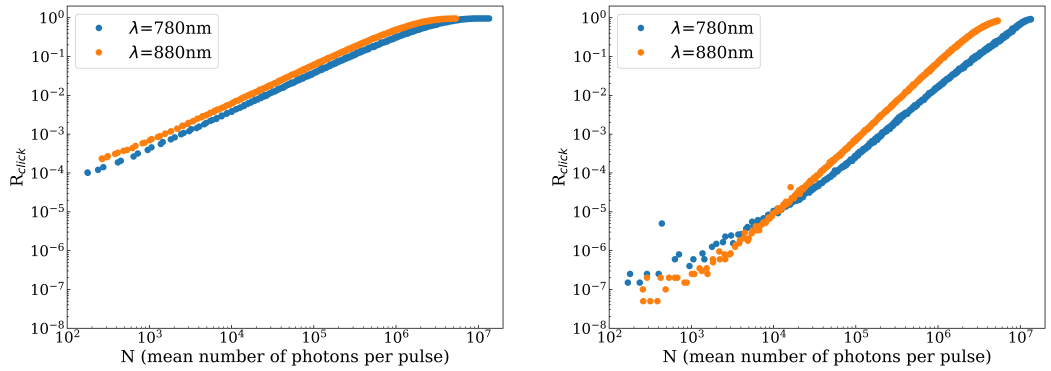

(a) (b)

Figure 8. Detector click probability R_{click} as a function of the mean number of photons per pulse N on the 100 nm wide NbTiN nanodetector for two wavelengths. Data are presented for two different bias currents (a) $I_b = 17.4$ μA and (b) $I_b = 11.1$ μA.

In contrast, at low bias current (figure 8(b)) the shape of the curves differs significantly revealing different photon contributions for each wavelength. At the lowest incident powers the 880 nm tomography curve presents lower detection rate when compared to the curve for 780 nm wavelength. At higher incident powers, where the multi photon processes are more dominant and the 880 nm curve presents a steeper slope, compared to the 780 nm curve. The shorter wavelength shows a tomography curve that starts with a slope corresponding to single-photon processes while the 880 nm wavelength data requires the inclusion of two-photon processes over the entire measurement range. These characteristics can easily be explained by the fact that the 880 nm photons have lower energy than the 780 nm ones. At lower powers, where the multi photon processes are improbable, fewer 880 nm photons are able to break superconductivity and lead to a detection event. At high powers the multi photon processes are more likely to happen and the count rate for 880 nm exceeds that of 780 nm.

As a final note it should be remarked that the highly anisotropic nanowires often show a pronounced polarization dependence in their optical response. To verify this polarization dependent response a half wave plate was placed just before the sample in order to explore the polarization dependent photon response. When varying the orientation of this second half wave plate different states of linearly polarized light are send to the SSPD. After the data analysis, no appreciable polarization dependence is observed in the tomography curves.

4. Conclusions

We have performed quantum detector tomography on three NbTiN nano-SSPD single photon detectors of 70, 100 and 150 nm width and successfully separated the detector response in single and multiple photon contributions. The tomography curves present unexpectedly large differences in the behaviour of the three detectors. Most notably, the 150 nm wide detector does not show a clear one photon regime nor saturation of the tomography curve observed for the 70 and 100 nm detector. In addition, the results for the 70 nm detector contain a strange drop of the counts at high powers that we tentatively attribute to local heating. This heating effect is currently poorly understood.

Furthermore, we have studied the energy dependent photon response of the 100 nm detector analyzing the shape of the tomography curves at two different wavelengths. Due to the non-linearity of these NbTiN devices, the full tomography treatment is needed in order to properly

compare the different wavelengths. Our results show that the internal efficiency of the 100 nm wide detector is lower for 880 nm wavelength photon detection compare to photon detection at 780 nm wavelength. Due to the design of the detector photon absorption at 880 nm is more efficient.

We have shown that the one photon regime occurs at very different current density depending on the width of the detector. The experimental results demonstrate that a wider detector is less efficient compared to a more narrow detector at similar current density.

Acknowledgments
I would like to thank my advisor M. J. A. de Dood for his continuous guidance and assistance during this project. Many thanks as well to my family and friends for their personal support and encouragement. This project has been made possible by financial support from the Gorter stichting.

References

[1] Gol'tsman G N, Okunev O, Chulkova G, Lipatov A, Semenov A, Smirnov K, Voronov B, Dzardanov A, Williams C and Sobolewski R 2001 Picosecond superconducting single-photon optical detector *Appl. Phys. Lett.* **79** 705-7
[2] Natarajan C M, Tanner M G and Hadfield R H 2012 Superconducting nanowire single-photon detectors: physics and applications *Supercond. Sci. Technol.* **25** 063001
[3] Kornev A, Korneeva Yu, Florya I, Voronov B and Gol'tsman G 2012 NbN nanowire superconducting single-photon detector for mid-infrared *Phys. Procedia* **36** 72-6
[4] Renema J J, Gaudio R, Wang Q, Zhou Z, Gaggero A, Mattioli F, Leoni R, Sahin D, de Dood M J A, Fiore A and van Exter M P 2014 Experimental test of theories of the detection mechanism in a nanowire superconducting single photon detector *Phys. Rev. Lett.* **112** 117604
[5] Berggren K K, Zhao Q, Abebe N, Chen M, Ravindran P, McCaughan A and Bardin J C 2018 A superconducting nanowire can be modeled by using SPICE *Supercond. Sci. Technol.* **31** 055010
[6] Skocpol W J, Beasley M R and Tinkham M 1974 Self-heating hotspots in superconductive thin-film microbridges *J. Appl. Phys.* **45** 4054
[7] Kerman A J, Dauler E A and Keicher W E 2006 Kinetic-inductance-limited reset time of superconducting nanowire photon counters *Appl. Phys. Lett.* **88** 1111116
[8] Bitauld D, Marsili F, Gaggero A, Mattioli F, Leoni R, Nejad S J, Lévy F and Fiore A 2010 Nanoscale optical detector with single-photon and multiphoton sensitivity *Nano. Lett.* **10** 2977-81
[9] Renema J J, Frucci G, de Dood M J A, Gill R, Fiore A and van Exter M P 2012 Tomography and state reconstruction with superconducting single-photon detectors *Phys. Rev. A* **86** 062113
[10] Wang Q, Renema J J, Gaggero A, Mattioli F, Leoni R, van Exter M P and de Dood M J A 2015 How noise affects quantum detector tomography *J. Appl. Phys.* **118** 134501
[11] Lundeen J S, Feito A, Coldenstrodt-Ronge H, Pregnell K L, Silberhorn Ch, Ralph T C, Eisert J, Plenio M B and Walmsley I A 2009 Tomography of quantum detectors *Nat. Phys.* **5** 27-30
[12] Renema J J, Wang Q, Gaudio R, Komen I, op't Hoog K, Sahin D, Schilling A, van Exter M P, Fiore A, Engel A and de Dood M J A 2015 Position-dependent local detection efficiency in a nanowire superconducting single-photon detector *Nano Lett.* **15** 4541-45
[13] Annunziata A J, Santavicca D F, Frunzio L, Catelani G, Rooks M J, Frydman A and Prober D E 2010 Tunable superconducting nanoinductors *Nanotechnology* **21** 445202
[14] Liu D K, You L X, Chen S J, Yang X Y, Wang Z, Wang Y L, Xie X M and Jiang M H 2013 Electrical characteristics of superconducting single photon detector *IEEE Trans. Appl. Supercond.* **23** 2200804
[15] Kerman A J, Yang J K W, Molnar R J, Dauler E A Berggren K K 2009 Electrothermal feedback in superconducting nanowire single-photon detectors *Phys. Rev. B* **79** 100509
[16] Caloz M, Korzh B, Timoney N, Weiss M, Garriglio S, Warburton R J, Schönenberger, Renema J, Zbinden H and Brussières F 2017 Optically probing the detection mechanism in a molybdenum silicide superconducting nanowire single-photon detector *Appl. Phys. Lett.* **110** 083106